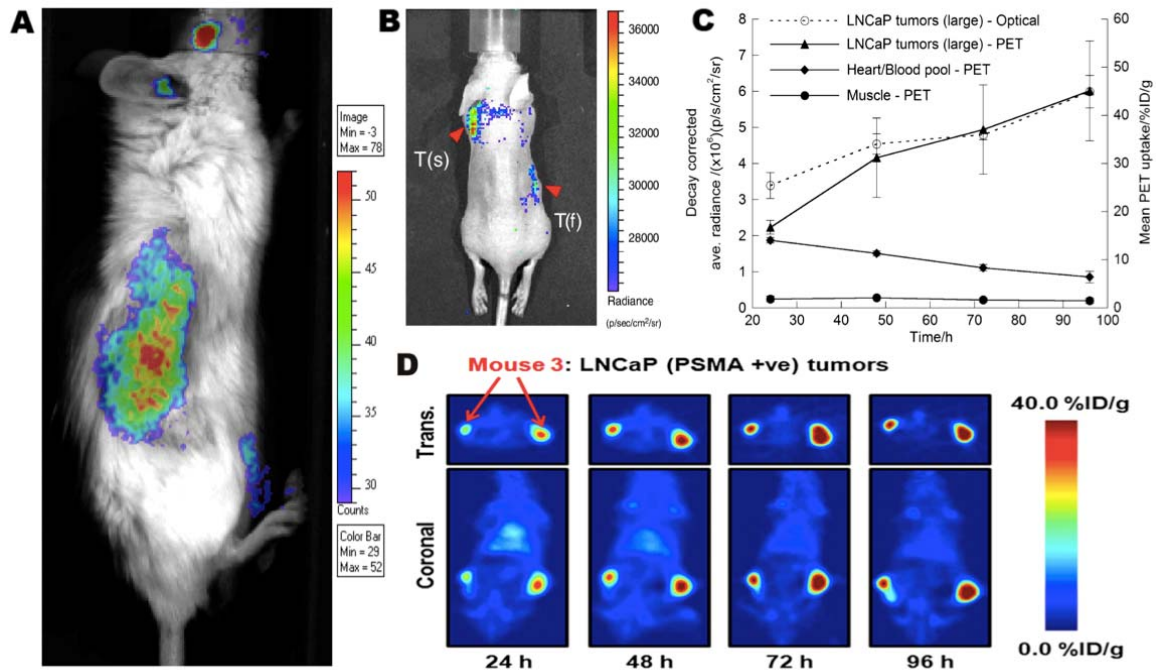
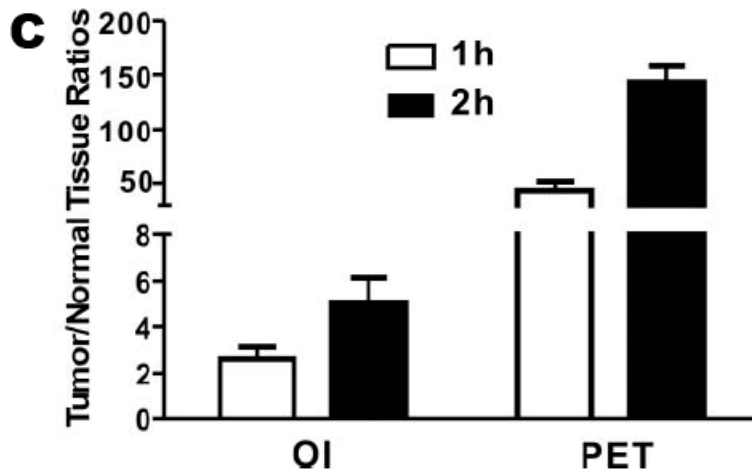
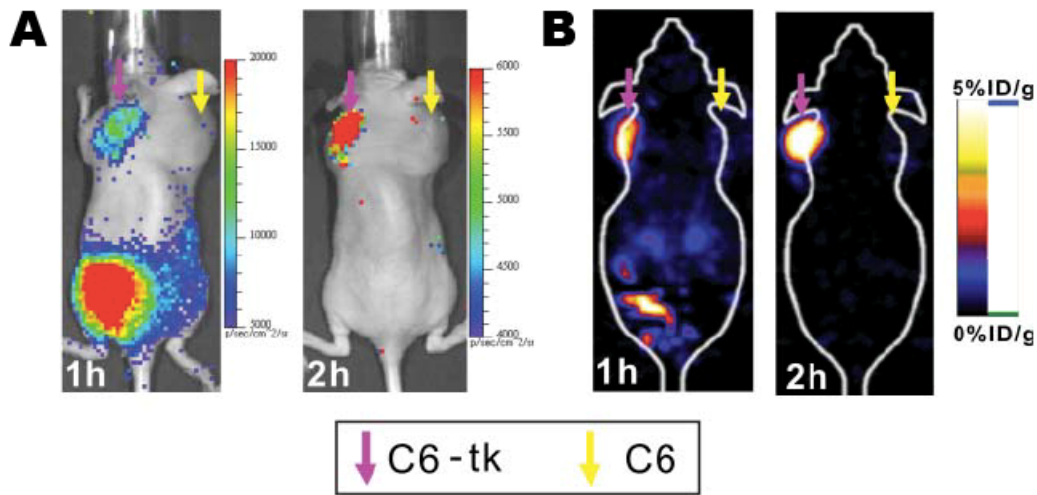


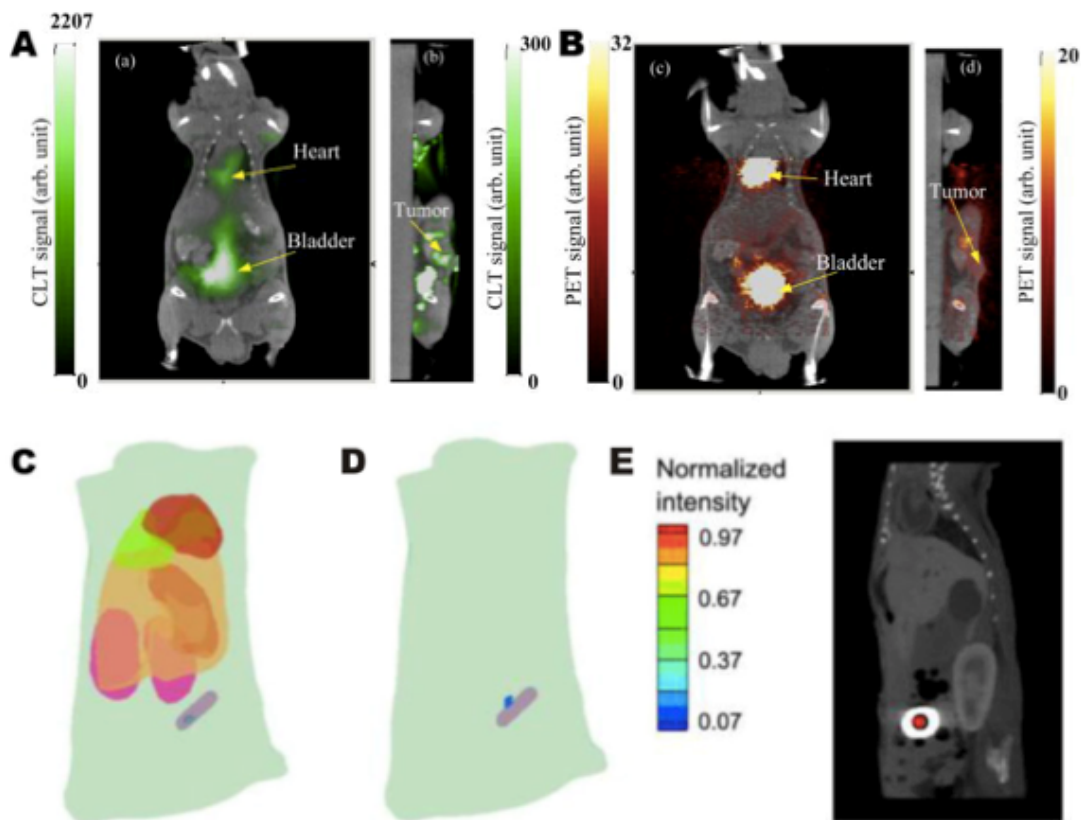
Supplemental Figure 1. *In vivo* radioactive OI of ¹⁸F-FDG in comparison with microPET. (A) Bioluminescence image of a nude mouse bearing C6-FLuc tumor. (B,C) Radioactive OI and microPET imaging of a nude mouse bearing C6-FLuc tumor injected via tail vein with ¹⁸F-FDG at 0.5, 1, 2 h p.i. (D) Radioactive OI of a normal mouse at 0.5, 1, 12, 24h after injection of Na¹³¹I via tail vein. (E) Radioactive OI of ⁹⁰Y-RGD-BBN in mice bearing PC3 tumor. (F–H) Quantitative analysis of radioactive OI (F) and microPET (G) results and their correlation (H) (adapted with permission from (12)).



Supplemental Figure 2. *In vivo* tumor imaging. **(A)** Optical scan of a mouse bearing a CWR22-RV1 xenograft following injection of 270 μCi FDG. Luminescence was detected throughout the animal, which is consistent with the broad distribution of FDG; however, for display, the image is thresholded to highlight the tumor region. In the tumor, the measured luminescence is $11\times$ the signal measured in a region above the tumor and $47\times$ the signal from the image background. **(B)** Luminescence imaging of a nude mouse bearing NIH3T6.7 tumor cells at 2 days after injection of ^{124}I -labeled Herceptin (3.29 MBq) by tail vein. The tumor regions are indicated by red arrowheads. Scan time is 1 min. **(C)** Temporal images of ^{89}Zr -DFO-J591 uptake (10.9–11.3 MBq [295–305 μCi], 60–62 μg of mAb, in 200 μL of 0.9% sterile saline) recorded in dual subcutaneous LNCaP (PSMA-positive) tumor-bearing severe combined immune deficient mouse between 24 and 96 h after administration. Images shown are coronal and transverse immune-PET images recorded for mouse 3 of a group of 3 mice. **(D)** Time-activity curves showing ROI and volume-of-interest analysis of CLI and immune-PET images for ^{89}Zr -DFO-J591 uptake in well-established (large) LNCaP tumors. Volume-of-interest analysis of immune-PET images shows change in ^{89}Zr activity in heart-blood pool and muscle tissue. ((A) adapted with permission from (9); (B) adapted with permission from (15); (C) and (D) adapted with permission from (14)).



Supplemental Figure 3. *In vivo* imaging using OI and PET. Mice bearing C6-tk and C6 tumors can be imaged by both (A) OI and (B) PET. (C) Statistical analysis was performed for both modalities ($n = 6$) (adapted with permission from (13)).



Supplemental Figure 4. Cerenkov Luminescence Tomography. (A-B) Reconstructed Cerenkov luminescence tomography images fused with microCT images: (A) (left) coronal cross section showing bladder and heart and (right) sagittal cross section at tumor. (B) Corresponding fused microPET/CT images. (C-E) CLT reconstruction of the radioactive source distribution in the mouse with an implanted $600 \mu\text{Ci Na}^{131}\text{I}$ radioactive source. (C) and (D) are the 3D renderings of the reconstructed source distribution in heterogeneous and homogeneous mouse models respectively. (E) The true source (inside the black circle) in a micro-CT slice superimposed with the reconstructed source (red triangle) from a sagittal view ((A-B) adapted with permission from (30); (C-E) adapted with permission from (16)).